ACS OMEGA

http://pubs.acs.org/journal/acsodf

Article

Controlled Transformation of Liquid Metal Microspheres in Aqueous Solution Triggered by Growth of GaOOH

Xiaofei Li, Xin Ding, Yuhang Du, Chao Xiao, Kang Zheng, Xianglan Liu, Xingyou Tian, and Xian Zhang*

Cite This: *ACS Omega* 2022, 7, 7912–7919

Read Online

ACCESS | Metrics & More | Article Recommendations | Supporting Information

ABSTRACT: Liquid metals (LMs) are playing an increasingly important role in the fields of flexible devices, electronics, and thermal management due to their low melting point and excellent thermal and electrical conductivity, and the transformation of LMs in deionized water has recently received much attention. In this paper, we investigate the transformation process of EGaIn microspheres in deionized water and propose a two-step process of microspherical transformation, whereby the microspheres are first deformed into a spindle shape and then into lamellar nanorods. It is also shown that the growth of GaOOH crystals drives the transformation. Based on this result, EGaIn microspheres with controllable transformation could be prepared, such as spindle or lamellar rod shapes, extending the application area of LMs.

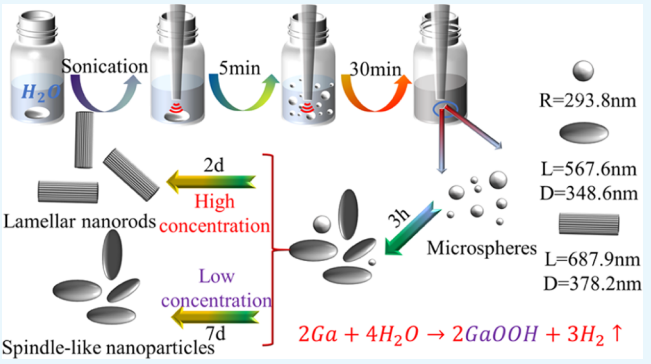

INTRODUCTION

Liquid metals (LMs) are metals with melting points of below or near room temperature,[1−3] and as a kind of LM, Ga has the advantages of low melting point (29.7 °C), low toxicity,[4] low viscosity,[5] excellent conductivity,[6] and thermal conductivity.[7] In addition, the melting point temperature of gallium-based alloys such as gallium indium alloy (EGaIn),[8] gallium tin alloy (EGaSn), and gallium indium tin alloy (EGaInSn, Galinstan) can be regulated by changing the proportion of alloy components. These unique properties of gallium-based LMs make them have wide application potential in soft electronics,[1,9,10] flexible devices,[11,12] biological devices,[13,14] thermal management,[15,16] and nuclear industry.[17,18]

Gallium-based LMs are highly susceptible to oxidation when exposed to air, forming a dense thin film of gallium oxide, which prevents further oxidation of internal gallium[1,19] while reducing the surface tension,[20] thermal conductivity, and conductivity of LM.[21,22] However, a significant morphological change occurs when LM is dispersed in deionized (DI) water to form LM microspheres. Porat's group[23] sonicated pure gallium in DI water and found the presence of GaOOH microcrystals on the surface of gallium microspheres. Dickey's group[24] dispersed gallium indium alloy in DI water to form the LM microsphere suspension using an ultrasonic probe, investigated the process of LM microsphere transformation from microspheres to nanorods, proved that heating makes EGaIn microspheres turn into GaOOH lamellae, and drew a conclusion that heating promoted the transformation of LM microspheres. Then, Zhou's group[25] prepared LM microspheres with photoinduced transformation using a similar method. They dispersed EGaIn into microspheres in DI water and coated polydopamine (PDA) on the surface, using the photothermal conversion ability of PDA to control the transformation of LM microspheres; however, LM microspheres can only deform into spindle-like particles unlike Dickey group's report. In addition, Kalantar-Zadeh's group[26] prepared GaOOH by oxidizing pure gallium in DI water with the aid of ultrasound, where the surface of the gallium was oxidized in water, and the oxide layer prevented the oxidation of the internal gallium, which could be peeled off by ultrasound, thus oxidizing all the pure gallium into monolayer GaOOH crystals. In the present reports, similar conditions yielded different results and, in addition to the shape change, the components of the deformed LM also changed, thus supposedly resulting in properties different from pure gallium or gallium-based alloys with new functions.[22] However, there are few reports on the transformation mechanism and performance changes of LM microspheres in DI water. If the mechanism of transformation of LM microspheres in DI water can be investigated clearly, it is of great importance to guide the shape regulation of LM microspheres in water and to improve the stability of LM microspheres in DI water, and it

Received: December 6, 2021
Accepted: February 14, 2022
Published: February 23, 2022

can greatly expand the application fields of LM, for example, semiconductor,[27,28] catalyst,[29,30] drug delivery systems,[31,32] and so forth.

In view of this, we designed experiments to explore the transformation mechanism of LM microspheres in DI water and the material changes during transformation. A suspension of LM microspheres was prepared by successfully dispersing EGaIn in DI water under an ice−water bath using an ultrasonic cell disruptor,[33] as shown in Figure 1a. The suspension was then allowed to stand at room temperature and sampled at regular intervals. Surprisingly, it was found that the LM microspheres were transformed into a spindle shape and then into nanorods formed by stacking GaOOH sheet crystals face-to-face (Figure 1b), which has new applications as optics,[26,34] catalysts,[35,36] gallium oxide semiconductors,[22,37] and so on. Moreover, the final morphology in the spindle shape could be successfully stabilized by controlling the concentration of LM microspheres in the suspension. Finally, the mechanism of LM microspherical shape transformation was meticulously explored, and the whole transformation process was explained, providing a guide for improving the stability of LM water suspensions and obtaining LM microspheres with tunable shape, which has potential applications for the drug delivery system[4,38,39] and colloidal jamming.[40]

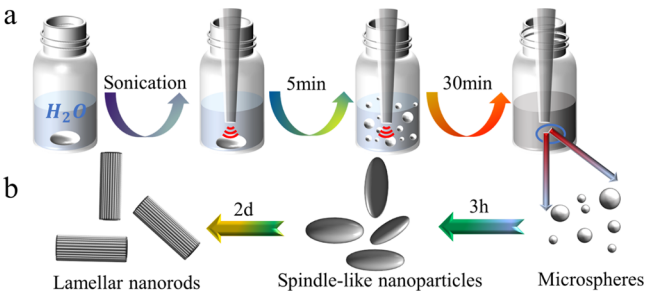

Figure 1. (a) EGaIn was added to DI water and ultrasonically crushed for 30 min to obtain an aqueous suspension of LM microspheres. (b) LM microspheres in the suspension are first deformed into a spindle shape and then into lamellar nanorods.

RESULTS AND DISCUSSION

Morphological Transformation of LM Microspheres. 0.2 g of EGaIn was added to 20 mL of DI water and then broken with an ultrasonical probe in ice−water bath for 30 min at 75 W.[25] The suspension was then centrifuged to obtain the LM nano droplet suspension with standard concentration. The suspensions were left to stand at room temperature and sampled regularly for observation. Different from the previous reports of direct transformation of LM microspheres into nanorods,[24] it was found that the transformation of LM microspheres includes two steps: the microspheres first become spindle-shaped, as shown in Figure 2(a2,a3). LM microspheres with an average size of 293.8 nm become spindle-like particles with an average length of 576.6 nm and

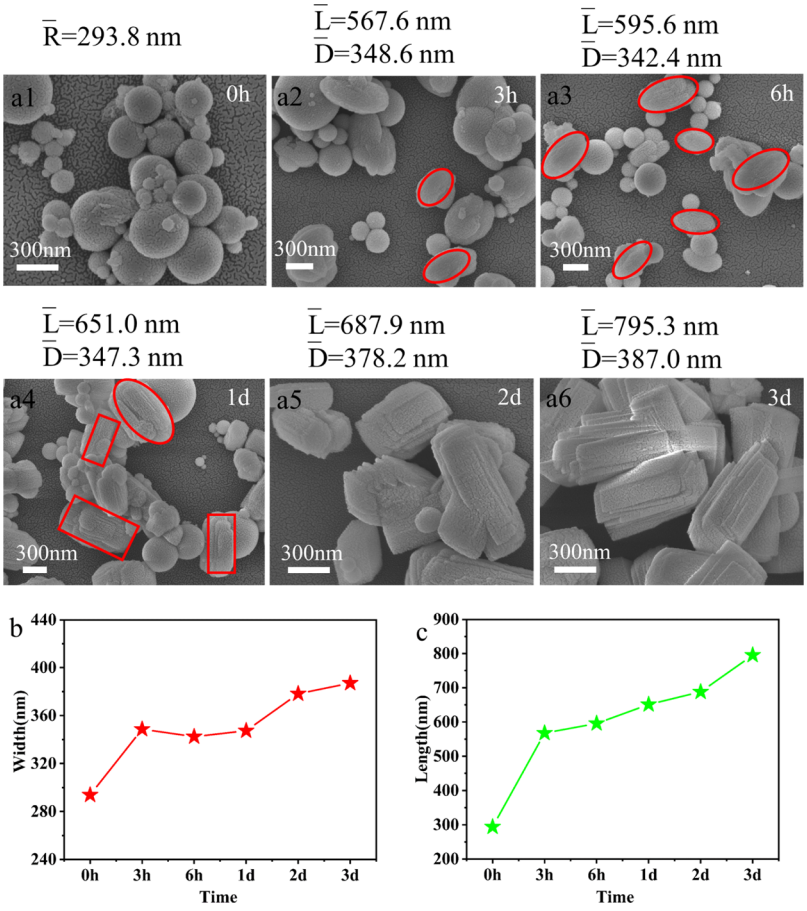

Figure 2. (a) Morphology and particle size of LM particles at 0 h, 3 h, 6 h, 1 day, 2 days, and 3 days. (b,c) Plot of the variation of the width and length of LM particles during transformation.

https://doi.org/10.1021/acsomega.1c06897
ACS Omega 2022, 7, 7912−7919

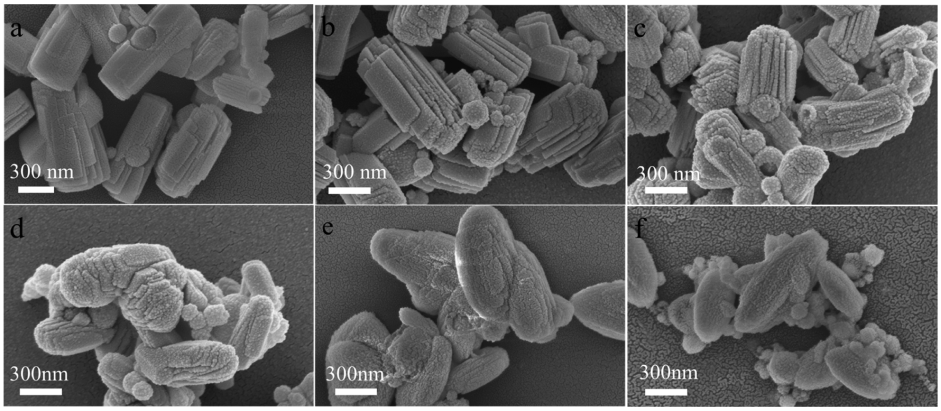

Figure 3. Morphology of particles in a suspension of standard concentration diluted (a) 0 times, (b) 2.5 times, (c) 7.5 times, (d) 15 times, (e) 30 times, and (f) 60 times and maintained for 3 days.

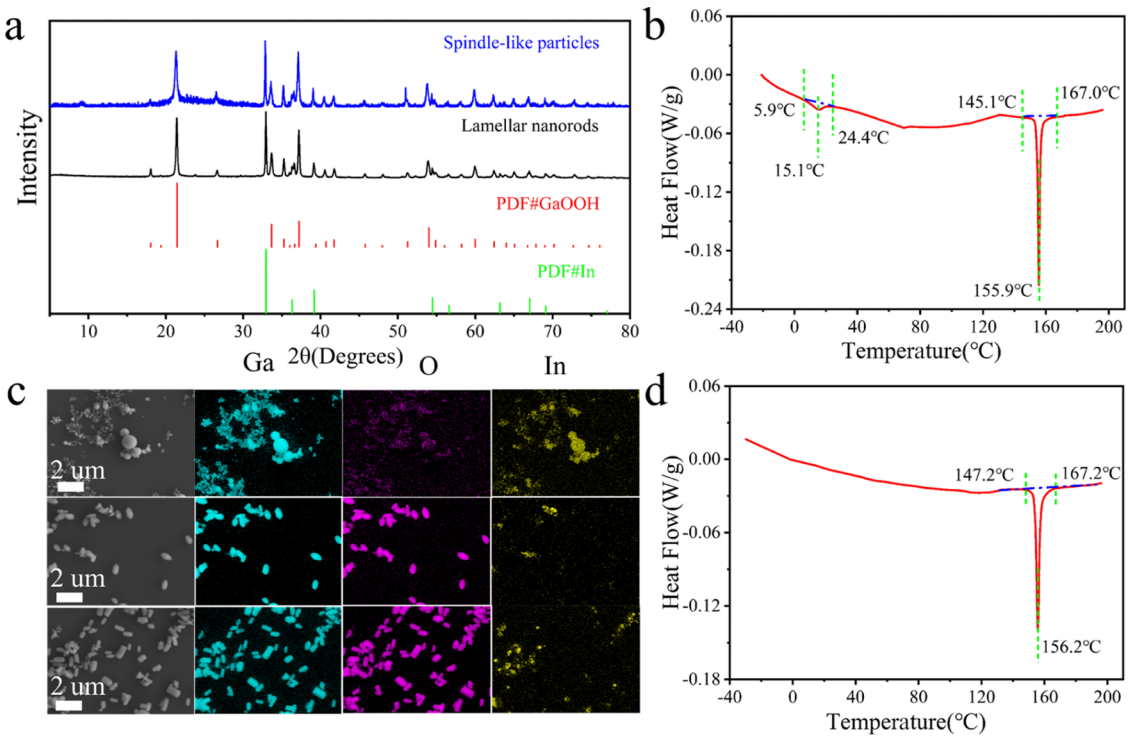

Figure 4. (a) XRD spectra of the spindle-like particles and the lamellar nanorods and the spectra for standard GaO_2H (PDF #06-0180) and In (PDF #05-0642). (b) DSC curves of spindle-like particles obtained after resting for 12 h. (c) SEM images and EDS mappings of the microsphere, the spindle-like particles, and the lamellar nanorods. (d) DSC curves of lamellar nanorods.

an average width of 348.6 nm after 3 h. At 6 h, the average length and width of the spindle-like particles are 595.6 and 342.4 nm, respectively, and their particle size distribution is shown in Figure S1. Then, the spindle-like particles are deformed into lamellar nanorods, as shown in Figure 2(a4); in this case, the average length of the particles is 651.0 nm, the average width is 347.3 nm, and the particle size distribution is shown in Figure S2. On the second day, the particles are basically transformed into lamellar nanorods, and the average length and width of the nanoparticles are 687.9 and 378.2 nm, respectively. The lamellar nanorods are still growing at this time, the average length and width of the lamellar nanorods are 795.3 and 387.0 nm, respectively, on the third day, as shown in Figure 2(a6), and the particle size distribution is shown in Figure S3. In addition, it can be found in Figure 2b,c that the average length and width of the particles increased during the transformation process; however, the length increased faster and grew preferentially in the length direction from 3 h to day 1.

LM microspheres in DI water eventually turn into lamellar nanorods. To address this issue, we explored the factors affecting the morphology of LM microspheres in DI water. After experiments, it was found that the concentration of LM microspheres determined the final shape of microspheres. When the suspension of the standard concentration was, respectively, diluted 2.5 and 7.5 times, LM microspheres will still deform into laminar nanorods after resting for 3 days, as shown in Figure 3b,c. When diluted 15 times, the nanosheets that make up the nanorods were no longer regular, and the final morphology had transitioned to a spindle shape, as shown in Figure 3d. However, when the dilution level reached 30 times, the final morphology stayed in a spindle shape, although

https://doi.org/10.1021/acsomega.1c06897
ACS Omega 2022, 7, 7912−7919

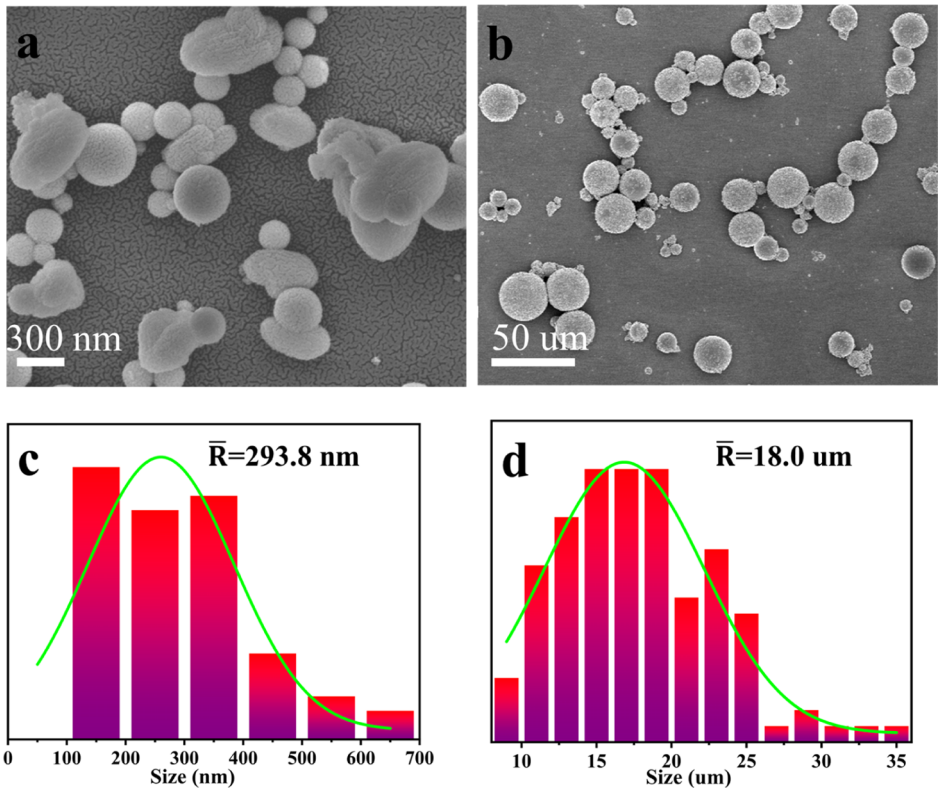

Figure 5. (a) After standing for 6 h, some of the microspheres became spindle-like. (b) After treatment with NaOH solution, the particles were transformed into microspheres. (c) Particle size distribution of the freshly prepared EGaIn microspheres, the average particle size of the microspheres is 293.8 nm. (d) Particle size distribution of the microspheres obtained after NaOH treatment, the average particle size of the microspheres is 18.0 μm.

the nanosheets could still be observed on its surface, as shown in Figure 3e. At a dilution of 60 times, the microspheres disappeared, and the final form was spindle-like, as shown in Figure 3f. The suspensions of standard concentrations and different dilutions are shown in Figure S4, and the particles precipitated after 3 days of standing. In order to avoid the error caused by a too short resting time, the resting time was extended, and the results were similar (Figure S5). According to this result, the morphology of LM microspheres could be regulated by controlling the suspension concentration and resting time. In the meantime, we performed X-ray diffraction (XRD) analysis of the particles stabilized in both morphologies separately, as shown in Figure 4a. The main components of the particles in both forms are GaOOH (GaO_2H). Differential scanning calorimetry (DSC) was performed on the spindle-like particles obtained at 12 h and the lamellar nanorods obtained at 3 days, as shown in Figure 4b,d. EGaIn was still present in the spindle-like particles at this time, and the heat absorption peak when indium melts could be observed; while in the DSC curve of the lamellar nanorods, there is no longer a heat absorption peak when EGaIn melts, but only a heat absorption peak when indium melts, which indicates that the indium is removed from the alloy, as shown in Figure 4c. The indium element is enriched into indium microspheres, detached from spindle-like particles and nanorods. This is consistent with previous reports on dealloying of EGaIn.[24]

Mechanism of the First Step of Transformation. According to the previous result, the first step in the transformation of EGaIn microspheres is that the microspheres change into spindle-like nanoparticles. During the resting process, it can be observed that the particles in the suspension precipitate, while generating many bubbles (Figure S6). In addition, LM can easily react with oxygen to form an amorphous gallium oxide film on its surface, with a thickness of about 2−3 nm.[41] As shown in Figure S7, the thickness of the amorphous oxide on the surface of the freshly prepared LM microspheres is 6 nm, much greater than that reported in the literature, which may be caused by the partial conversion of Ga_2O_3 to GaOOH. In view of the eventual product GaOOH, the reaction equation[42] is

$$4Ga + 3O_2 \rightarrow 2Ga_2O_3$$

$$Ga_2O_3 + H_2O \rightarrow 2GaOOH$$

$$2Ga + 4H_2O \rightarrow 2GaOOH + 3H_2\uparrow$$

We therefore conjecture that the GaOOH triggered transformation. In order to verify this conjecture, NaOH aqueous solution was added to the suspension that had been left for 6 h to remove GaOOH from the surface of particles,[43] and the spindle-like nanoparticles disappeared from the suspension after treatment, and the precipitated particles were microspheres with an average particle size of 18.0 μm, as shown in Figure 5a−c, which confirmed the conjecture that GaOOH brought about transformation. In addition, we found that the particles in the suspension treated by NaOH completely precipitated in about 40 min, while the untreated suspension has no obvious changes, as shown in Figure S8, indicating that GaOOH can slow down the sedimentation rate of particles.[44]

In order to further explore the mechanism of action of GaOOH, TEM was conducted for the particles in the suspension that stood for 6 h. As shown in Figure 6a, it can

https://doi.org/10.1021/acsomega.1c06897
ACS Omega 2022, 7, 7912−7919

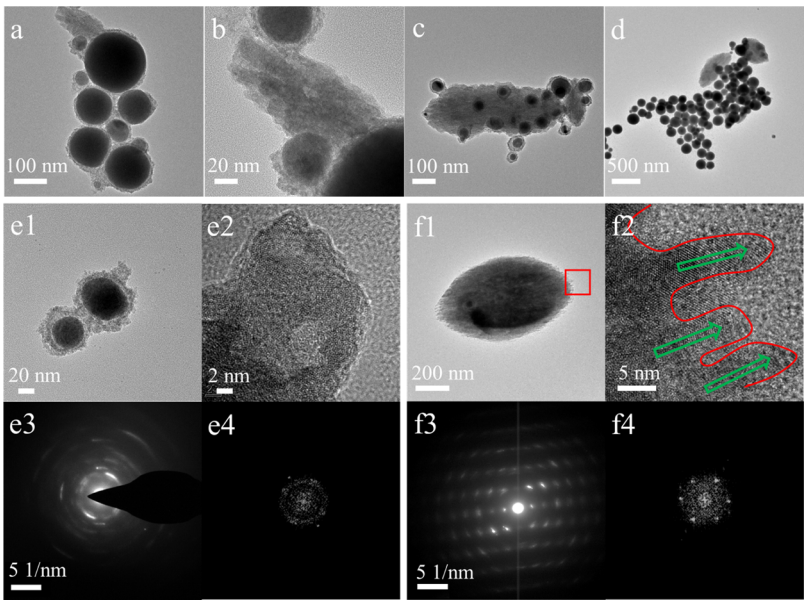

Figure 6. TEM images of the nanoparticles after standing for 6 h. (a,b) Outward growth of GaOOH crystals on the surface of microspheres. (c) Multiple small microspheres were in contact with each other through GaOOH and provide gallium atoms for the growth of GaOOH crystals. (d) Due to the presence of GaOOH on the surface, the microspheres did not fuse with each other. (e) TEM image of the microspheres (e1), HRTEM image of GaOOH on the surface of the microsphere (e2), FFT image of HRTEM (e3), and SEAD image of GaOOH on the surface of the microsphere (e4). (f) TEM image of a spindle-like particle (f1), HRTEM image of a spindle-like particle (f2), FFT image of HRTEM (f3), and SEAD image of a spindle-like particle (f4).

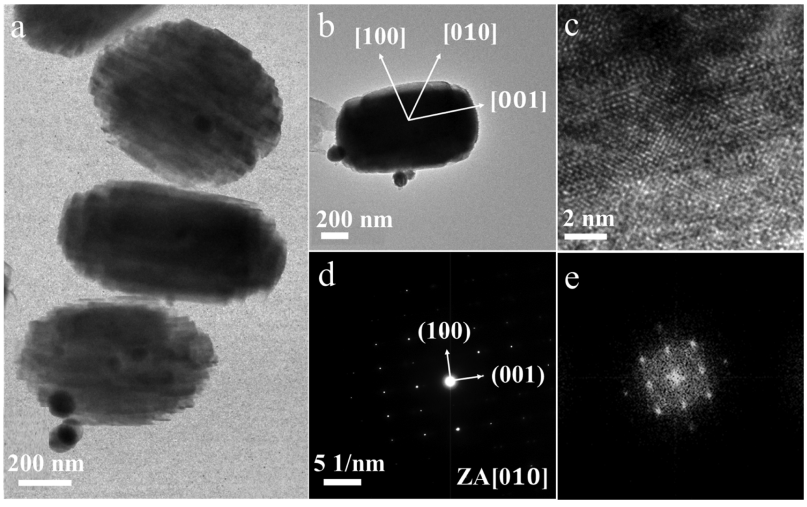

Figure 7. (a,b) TEM image of the lamellar nanorods. (c) HRTEM image of the lamellar nanorods. (d) SEAD pattern from the region of (b). (e) FFT image of the HRTEM image in (c).

be clearly observed that there is a layer of material on the surface of EGaIn microspheres. Combined with the previous result (Figure 4a,b), this layer of material is GaOOH. EGaIn microspheres will contact each other due to clusters, but GaOOH will hinder the fusion of EGaIn microspheres (Figure 6d) and slow down the precipitation rate, which is consistent with our previous experimental results (Figure S8). With the continuous outward growth of GaOOH on the surface of microspheres, spindle-like GaOOH nanoparticles will be gradually formed, as shown in Figure 6b. At the same time, small microspheres will contact each other by GaOOH and grow into a GaOOH particle during GaOOH growth, as shown in Figure 6c, which just explains why the size of microspheres changes greatly after transformation. The average particle size of microspheres before transformation is 293.8 nm, as shown in Figure 5d, while the average length and width of spindle-like particles are 595.6 and 342.4 nm, as shown in Figures 2(a3) and S1b.

In addition, we compared the high-resolution transmission electron microscopy (HRTEM) and selected-area electron diffraction (SEAD) of spindle-like particles and microspheres that had been left to stand for 6 h, further confirming that it was the growth of GaOOH that caused the transformation. As shown in Figure 6e, although HRTEM of the microspheres showed that there were crystalline regions of GaOOH, SEAD image and fast Fourier transform (FFT) of HRTEM demonstrated that GaOOH was not well crystallized. Compared to GaOOH of the microspheres' surface, the crystal structure of the spindle-like particles is more prefect,[45] as shown by the SEAD and FFT of HRTEM of the spindle

https://doi.org/10.1021/acsomega.1c06897
ACS Omega 2022, 7, 7912−7919

particles (Figure 6f). What is more, the EGaIn is still present in the spindle particles, as shown in Figure 4b. Furthermore, HRTEM of the edge region of the spindle particles shows that GaOOH is gradually growing in the direction of the long axis of the spindle (Figure 6f).[46,47] This is evidence that it is the growth of the GaOOH crystal that is causing the transformation.

Mechanism of the Second Step of Transformation. The further transformation of GaOOH spindle-like particles into GaOOH lamellar nanorods is to be explained in terms of the GaOOH crystal structure. We have performed TEM, HRTEM, and SEAD on the lamellar nanorods. As shown in Figure 7a, the lamellar nanorods are composed of lamellar GaOOH face-to-face stacking, which is consistent with the SEM results (Figure 2(a6)). HRTEM shows the crystal structure of GaOOH. Combining the SEAD and FFT of HRTEM, as shown in Figure 7b−d, the lamellar material is a single-crystal sheet of GaOOH, which belongs to the orthorhombic crystal system.[48] The length, width, and thickness of the sheet crystals are [001], [100], and [010] crystal orientations, respectively, as shown in Figure 7b. GaOOH is preferentially grown along the [001] direction, which is consistent with the previous reports[46,47] and explains why particles preferentially grow along their length (Figure 2b,c).

The crystal structure of GaOOH is similar to that of diaspore in that it consists of a double chain of co-edged octahedra, with gallium occupying two-thirds of the octahedral gap and the oxygen-hydroxy sheets arranged to form a closed hexagon.[49] In principle, the tighter the atomic arrangement of the crystalline surface, the lower the density of unsaturated bonds and therefore the lower the specific surface free energy.[50] Based on the gallium atomic density difference, the crystal planes with the lowest and highest surface energy are {010} and {001}, respectively. It has been demonstrated that the crystals preferentially grow in the [001] direction, similar to diaspore crystals, and the largest plane of the crystal shape at equilibrium belongs to the {010} plane.[47,49] Thus, lamellar nanorods consisting of GaOOH sheet crystal faces stacked on top of each other will be formed, and the lamellar rods no longer contain EGaIn this time, as shown in Figure 4d.

In combination with previous analysis, the EGaIn microspheres provide the gallium source for the growth of GaOOH crystals. First, GaOOH spindle-like particles are formed, and the crystals continue to grow until they are complete before forming GaOOH lamellar nanorods. However, if the concentration of EGaIn microspheres is too little to provide enough gallium atoms, they will not be able to form lamellar nanorods and stabilize in spindle or other shapes, which explains the results of Figure 3, and the concentration of EGaIn microspheres determines the final morphology. At the same time, gallium atoms are reduced due to depletion, and indium metal is gradually enriched, which in turn explains the dealloying phenomenon proposed by the previous report.[24]

CONCLUSIONS

In conclusion, this paper reports the detailed mechanism of the transformation of EGaIn microspheres in DI water, proposing a two-step process for the transformation of the microspheres. The first step is the oxidation of the microsphere surface to grow spindle-like GaOOH particles; the second step is that the microspheres act as a gallium source to provide gallium atoms to preferentially grow GaOOH along the [001] crystal orientation, which eventually deforms into nanorods made of GaOOH sheet crystal face-to-face stacks. It was also demonstrated the growth of GaOOH crystals that drives the transformation of the EGaIn microspheres. It provides guidance to improve the stability of LM microspheres in DI water and explains the dealloying phenomenon during LM transformation. In addition, this paper reports that the concentration of EGaIn microspheres can be used to regulate the final morphology of particles in water, achieving controlled transformation of EGaIn microspheres.

EXPERIMENTAL SECTION

Materials. EGaIn (LM) composed of 24.5% In and 75.5% Ga by weight was purchased from northeast nonferrous metals, and its melting point is 15.7 °C; DI water was prepared in our laboratory; NaOH (≥96%) was purchased from Tianjin BASF Chemical Co. Ltd.; and ethyl alcohol (99.5%) was purchased from Aladdin.

Preparation of the LM Suspension of Standard Concentration. 20 mL of DI water was poured into a glass reagent bottle, 0.20 g of EGaIn was added, and the system was ultrasonically treated for 30 min under ice−water bath with an ultrasonic cell disrupter (UX-300, Mitsui Electric Japan). After ultrasonic crushing, EGaIn was transformed into microspheres, and the LM suspension was obtained. However, the particle size of EGaIn microspheres was not uniform at this time. The suspension was centrifuged for 5 min at the speed of 2000 rad/min to remove EGaIn microspheres with excessive particle size. The suspension was then centrifuged for 8 min at a speed of 5000 rad/min to remove the nanoparticles with small particle size (HC-2518 high speed centrifuge, AnHui USTC Zonkia Scientific Instruments Co. Ltd.). Then, 1.5 mL of DI water was added to each centrifuge tube, which was removed after shocking evenly. Another 1 mL of DI water was added to the centrifuge tube for washing, and 20 mL of the LM suspension with standard concentration was finally obtained.

Characterization. The standard concentration of the suspension was diluted 2.5 times and placed in five small reagent bottles, and each bottle is about 10 mL. Samples were taken from the bottom of the sediment after standing for 0 h, 3 h, 6 h, 1 day, 2 days, and 3 days, respectively. SEM and energy-dispersive spectrometry (EDS) were performed after dilution (FIB, Auriga, Zeiss, Germany). Among them, samples were stood for 6 h and 3 days for HRTEM and SEAD (Tecnai TF-20, Thermo Fisher). The standard suspension was diluted 2.5, 7.5, 15, 30, and 60 times, respectively. 15 mL was taken from each group and placed in a small reagent bottle for 3 days and then sampled from the bottom for SEM. HRTEM and SEAD were also performed for samples diluted 30 times. The lamellar rod particles are obtained after dilution of 2.5 times, and the spindle particles are obtained after dilution of 30 times. The powders of the two groups of suspensions after drying at 120 °C (blast dryer, DHG-9075A, Shanghai Yiheng Scientific Instruments Co.) are for XRD (Rigaku SmartLab 9 kW, Japan Science Co.). 0.1 mol/L NaOH solution was added to the suspension that stood for 6 h and then stood for 40 min. The supernatant was poured out and cleaned with ethanol three times before sampling for SEM.

ASSOCIATED CONTENT

Supporting Information

The Supporting Information is available free of charge at https://pubs.acs.org/doi/10.1021/acsomega.1c06897.

https://doi.org/10.1021/acsomega.1c06897
ACS Omega 2022, 7, 7912−7919

Length and width distribution of the nanoparticles resting for 3 and 6 h; width and length distribution of the nanoparticles resting for 1, 2, and 3 d; suspensions of standard concentrations and dilutions of different magnitudes; nanoparticles precipitating after the suspension left to stand for 3 d; morphology of nanoparticles in a suspension of standard concentration diluted 2.5, 7.5, 15, 30, and 60 times and stood for 7 d; nanoparticles after ultrasonic crushing precipitating and producing a large number of bubbles in the suspension; oxide layer on the surface of LM microspheres of about 6 nm thickness; FFT diagram of HRTEM of the oxide layer; particles in the NaOH-treated suspension completely precipitating in about 40 min; and untreated suspensions not changing significantly within 40 min (PDF)

AUTHOR INFORMATION

Corresponding Author

Xian Zhang − *Key Laboratory of Photovoltaic and Energy Conservation Materials, Institute of Solid State Physics, HFIPS, Chinese Academy of Sciences, Hefei 230031, China; University of Science and Technology of China, Hefei 230026, People's Republic of China;* orcid.org/0000-0002-7910-1562; Email: xzhang@issp.ac.cn

Authors

Xiaofei Li − *Key Laboratory of Photovoltaic and Energy Conservation Materials, Institute of Solid State Physics, HFIPS, Chinese Academy of Sciences, Hefei 230031, China; University of Science and Technology of China, Hefei 230026, People's Republic of China*

Xin Ding − *Key Laboratory of Photovoltaic and Energy Conservation Materials, Institute of Solid State Physics, HFIPS, Chinese Academy of Sciences, Hefei 230031, China*

Yuhang Du − *Key Laboratory of Photovoltaic and Energy Conservation Materials, Institute of Solid State Physics, HFIPS, Chinese Academy of Sciences, Hefei 230031, China; University of Science and Technology of China, Hefei 230026, People's Republic of China*

Chao Xiao − *Key Laboratory of Photovoltaic and Energy Conservation Materials, Institute of Solid State Physics, HFIPS, Chinese Academy of Sciences, Hefei 230031, China*

Kang Zheng − *Key Laboratory of Photovoltaic and Energy Conservation Materials, Institute of Solid State Physics, HFIPS, Chinese Academy of Sciences, Hefei 230031, China;* orcid.org/0000-0003-0891-2808

Xianglan Liu − *Key Laboratory of Photovoltaic and Energy Conservation Materials, Institute of Solid State Physics, HFIPS, Chinese Academy of Sciences, Hefei 230031, China*

Xingyou Tian − *Key Laboratory of Photovoltaic and Energy Conservation Materials, Institute of Solid State Physics, HFIPS, Chinese Academy of Sciences, Hefei 230031, China; University of Science and Technology of China, Hefei 230026, People's Republic of China*

Complete contact information is available at: https://pubs.acs.org/10.1021/acsomega.1c06897

Notes

The authors declare no competing financial interest.

ACKNOWLEDGMENTS

The authors would like to acknowledge the financial support from the National Key Research and Development Program of China (no. 2017YFB0406200) and CASHIPS Director's Fund (YZJJZX202015).

REFERENCES

(1) Dickey, M. D. Emerging applications of liquid metals featuring surface oxides. *ACS Appl. Mater. Interfaces* **2014**, *6*, 18369−18379.

(2) Chen, Y.; Liu, Z.; Zhu, D.; Handschuh-Wang, S.; Liang, S.; Yang, J.; Kong, T.; Zhou, X.; Liu, Y.; Zhou, X. Liquid metal droplets with high elasticity, mobility and mechanical robustness. *Mater. Horiz.* **2017**, *4*, 591−597.

(3) Daeneke, T.; Khoshmanesh, K.; Mahmood, N.; de Castro, I. A.; Esrafilzadeh, D.; Barrow, S. J.; Dickey, M. D.; Kalantar-Zadeh, K. Liquid metals: fundamentals and applications in chemistry. *Chem. Soc. Rev.* **2018**, *47*, 4073−4111.

(4) Lu, Y.; Hu, Q.; Lin, Y.; Pacardo, D. B.; Wang, C.; Sun, W.; Ligler, F. S.; Dickey, M. D.; Gu, Z. Transformable liquid-metal nanomedicine. *Nat. Commun.* **2015**, *6*, 10066−10076.

(5) Spells, K. E. The determination of the viscosity of liquid gallium over an extended range of temperature. *Proc. Phys. Soc.* **1936**, *48*, 299−311.

(6) Bhuyan, P.; Wei, Y.; Sin, D.; Yu, J.; Nah, C.; Jeong, K.-U.; Dickey, M. D.; Park, S. Soft and Stretchable Liquid Metal Composites with Shape Memory and Healable Conductivity. *ACS Appl. Mater. Interfaces* **2021**, *13*, 28916−28924.

(7) Bartlett, M. D.; Kazem, N.; Powell-Palm, M. J.; Huang, X.; Sun, W.; Malen, J. A.; Majidi, C. High thermal conductivity in soft elastomers with elongated liquid metal inclusions. *Proc. Natl. Acad. Sci. U.S.A.* **2017**, *114*, 2143−2148.

(8) Dickey, M. D.; Chiechi, R. C.; Larsen, R. J.; Weiss, E. A.; Weitz, D. A.; Whitesides, G. M. Eutectic gallium-indium (EGaIn): A liquid metal alloy for the formation of stable structures in microchannels at room temperature. *Adv. Funct. Mater.* **2008**, *18*, 1097−1104.

(9) Lipomi, D. J.; Vosgueritchian, M.; Tee, B. C.-K.; Hellstrom, S. L.; Lee, J. A.; Fox, C. H.; Bao, Z. Skin-like pressure and strain sensors based on transparent elastic films of carbon nanotubes. *Nat. Nanotechnol.* **2011**, *6*, 788−792.

(10) Zhang, M.; Li, G.; Huang, L.; Ran, P.; Huang, J.; Yu, M.; Yuqian, H.; Guo, J.; Liu, Z.; Ma, X. Versatile fabrication of liquid metal nano-ink based flexible electronic devices. *Appl. Mater. Today* **2021**, *22*, 100903.

(11) Palleau, E.; Reece, S.; Desai, S. C.; Smith, M. E.; Dickey, M. D. Self-healing stretchable wires for reconfigurable circuit wiring and 3D microfluidics. *Adv. Mater.* **2013**, *25*, 1589−1592.

(12) Wu, P.; Zhou, L.; Lv, S.; Fu, J.; He, Y. Self-sintering liquid metal ink with LAPONITE for flexible electronics. *J. Mater. Chem. C* **2021**, *9*, 3070−3080.

(13) Jin, C.; Zhang, J.; Li, X.; Yang, X.; Li, J.; Liu, J. Injectable 3-D Fabrication of Medical Electronics at the Target Biological Tissues. *Sci. Rep.* **2013**, *3*, 3442−3449.

(14) Li, X.; Li, M.; Xu, J.; You, J.; Yang, Z.; Li, C. Evaporation-induced sintering of liquid metal droplets with biological nanofibrils for flexible conductivity and responsive actuation. *Nat. Commun.* **2019**, *10*, 3514−3523.

(15) Chang, J.; Zhang, Q.; Lin, Y.; Zhou, C.; Yang, W.; Yan, L.; Wu, G. Carbon Nanotubes Grown on Graphite Films as Effective Interface Enhancement for an Aluminum Matrix Laminated Composite in Thermal Management Applications. *ACS Appl. Mater. Interfaces* **2018**, *10*, 38350−38358.

(16) Yang, X.-H.; Tan, S.-C.; Liu, J. Thermal management of Li-ion battery with liquid metal. *Energy Convers. Manage.* **2016**, *117*, 577−585.

(17) Lazareva, S.; Ismagilov, Z.; Kuznetsov, V.; Shikina, N.; Kerzhentsev, M. Uranium oxide catalysts: environmental applications for treatment of chlorinated organic waste from nuclear industry. *Environ. Technol.* **2019**, *40*, 1881−1889.

(18) Guo, J.; Cheng, J.; Tan, H.; Zhu, S.; Qiao, Z.; Yang, J.; Liu, W. Al-Doped Ga-Based Liquid Metal: Modification Strategy and Controllable High-Temperature Lubricity through Frictional Interface Regulation. *Langmuir* **2019**, *35*, 6905−6915.
(19) Thelen, J.; Dickey, M. D.; Ward, T. A study of the production and reversible stability of EGaIn liquid metal microspheres using flow focusing. *Lab Chip* **2012**, *12*, 3961−3967.
(20) Sun, X.; Guo, R.; Yuan, B.; Chen, S.; Wang, H.; Dou, M.; Liu, J.; He, Z.-Z. Low-Temperature Triggered Shape Transformation of Liquid Metal Microdroplets. *ACS Appl. Mater. Interfaces* **2020**, *12*, 38386−38396.
(21) Handschuh-Wang, S.; Gan, T.; Wang, T.; Stadler, F. J.; Zhou, X. Surface Tension of the Oxide Skin of Gallium-Based Liquid Metals. *Langmuir* **2021**, *37*, 9017−9025.
(22) Lertanantawong, B.; Riches, J. D.; O'Mullane, A. P. Room Temperature Electrochemical Synthesis of Crystalline GaOOH Nanoparticles from Expanding Liquid Metals. *Langmuir* **2018**, *34*, 7604−7611.
(23) Kumar, V. B.; Gedanken, A.; Kimmel, G.; Porat, Z. Ultrasonic cavitation of molten gallium: formation of micro- and nano-spheres. *Ultrason. Sonochem.* **2014**, *21*, 1166−1173.
(24) Lin, Y.; Liu, Y.; Genzer, J.; Dickey, M. D. Shape-transformable liquid metal nanoparticles in aqueous solution. *Chem. Sci.* **2017**, *8*, 3832−3837.
(25) Gan, T.; Shang, W.; Handschuh-Wang, S.; Zhou, X. Light-Induced Shape Morphing of Liquid Metal Nanodroplets Enabled by Polydopamine Coating. *Small* **2019**, *15*, No. e1804838.
(26) Syed, N.; Zavabeti, A.; Mohiuddin, M.; Zhang, B.; Wang, Y.; Datta, R. S.; Atkin, P.; Carey, B. J.; Tan, C.; van Embden, J.; Chesman, A. S. R.; Ou, J. Z.; Daeneke, T.; Kalantar-Zadeh, K. Sonication-Assisted Synthesis of Gallium Oxide Suspensions Featuring Trap State Absorption: Test of Photochemistry. *Adv. Funct. Mater.* **2017**, *27*, 1702295.
(27) Jiang, Y.; Tian, B. Inorganic semiconductor biointerfaces. *Nat. Rev. Mater.* **2018**, *3*, 473−490.
(28) Carey, B. J.; Ou, J. Z.; Clark, R. M.; Berean, K. J.; Zavabeti, A.; Chesman, A. S. R.; Russo, S. P.; Lau, D. W. M.; Xu, Z.-Q.; Bao, Q.; Kavehei, O.; Gibson, B. C.; Dickey, M. D.; Kaner, R. B.; Daeneke, T.; Kalantar-Zadeh, K. Wafer-scale two-dimensional semiconductors from printed oxide skin of liquid metals. *Nat. Commun.* **2017**, *8*, 14482−14491.
(29) Tzani, M. A.; Kallitsakis, M. G.; Symeonidis, T. S.; Lykakis, I. N. Alumina-Supported Gold Nanoparticles as a Bifunctional Catalyst for the Synthesis of 2-Amino-3-arylimidazo[1,2-a]pyridines. *ACS Omega* **2018**, *3*, 17947−17956.
(30) Liang, S.-T.; Wang, H.-Z.; Liu, J. Progress, Mechanisms and Applications of Liquid-Metal Catalyst Systems. *Chem.—Eur. J.* **2018**, *24*, 17616−17626.
(31) Xu, X.; Yang, G.; Xue, X.; Lu, H.; Wu, H.; Huang, Y.; Jing, D.; Xiao, W.; Tian, J.; Yao, W.; Pan, C.-x.; Lin, T.-y.; Li, Y. A polymer-free, biomimicry drug self-delivery system fabricated via a synergistic combination of bottom-up and top-down approaches. *J. Mater. Chem. B* **2018**, *6*, 7842−7853.
(32) Sun, X.; Sun, M.; Liu, M.; Yuan, B.; Gao, W.; Rao, W.; Liu, J. Shape tunable gallium nanorods mediated tumor enhanced ablation through near-infrared photothermal therapy. *Nanoscale* **2019**, *11*, 2655−2667.
(33) Lebon, G. S. B.; Tzanakis, I.; Pericleous, K.; Eskin, D.; Grant, P. S. Ultrasonic liquid metal processing: The essential role of cavitation bubbles in controlling acoustic streaming. *Ultrason. Sonochem.* **2019**, *55*, 243−255.
(34) Kominami, H.; Kitagawa, S.-y.; Okubo, Y.; Fukui, M.; Hashimoto, K.; Imamura, K. Organically modified titania having a metal catalyst: a new type of liquid-phase hydrogen-transfer photocatalyst working under visible light irradiation and H2-free conditions. *Phys. Chem. Chem. Phys.* **2016**, *18*, 16076−16079.
(35) Sun, M.; Li, D.; Zhang, W.; Fu, X.; Shao, Y.; Li, W.; Xiao, G.; He, Y. Rapid microwave hydrothermal synthesis of GaOOH nanorods with photocatalytic activity toward aromatic compounds. *Nanotechnology* **2010**, *21*, 355601.
(36) Zhang, W.; Naidu, B. S.; Ou, J. Z.; O'Mullane, A. P.; Chrimes, A. F.; Carey, B. J.; Wang, Y.; Tang, S.-Y.; Sivan, V.; Mitchell, A.; Bhargava, S. K.; Kalantar-Zadeh, K. Liquid metal/metal oxide frameworks with incorporated Ga2O3 for photocatalysis. *ACS Appl. Mater. Interfaces* **2015**, *7*, 1943−1948.
(37) Lee, M.-L.; Mue, T. S.; Huang, F. W.; Yang, J. H.; Sheu, J. K. High-performance GaN metal−insulator−semiconductor ultraviolet photodetectors using gallium oxide as gate layer. *Opt. Express* **2011**, *19*, 12658−12663.
(38) Kim, D.; Hwang, J.; Choi, Y.; Kwon, Y.; Jang, J.; Yoon, S.; Choi, J. Effective Delivery of Anti-Cancer Drug Molecules with Shape Transforming Liquid Metal Particles. *Cancers* **2019**, *11*, 1666−1678.
(39) Zhang, J.; Guo, R.; Liu, J. Self-propelled liquid metal motors steered by a magnetic or electrical field for drug delivery. *J. Mater. Chem. B* **2016**, *4*, 5349−5357.
(40) Donev, A.; Connelly, R.; Stillinger, F. H.; Torquato, S. Underconstrained jammed packings of nonspherical hard particles: Ellipses and ellipsoids. *Phys. Rev. E: Stat., Nonlinear, Soft Matter Phys.* **2007**, *75*, 051304.
(41) Ren, L.; Zhuang, J.; Casillas, G.; Feng, H.; Liu, Y.; Xu, X.; Liu, Y.; Chen, J.; Du, Y.; Jiang, L.; Dou, S. X. Nanodroplets for Stretchable Superconducting Circuits. *Adv. Funct. Mater.* **2016**, *26*, 8111−8118.
(42) Hu, Y.; Zhuo, H.; Zhang, Y.; Lai, H.; Yi, J.; Chen, Z.; Peng, X.; Wang, X.; Liu, C.; Sun, R.; Zhong, L. Graphene Oxide Encapsulating Liquid Metal to Toughen Hydrogel. *Adv. Funct. Mater.* **2021**, *31*, 2106761.
(43) Yi, L.; Ding, Y.; Yuan, B.; Wang, L.; Tian, L.; Chen, C.; Liu, F.; Lu, J.; Song, S.; Liu, J. Breathing to harvest energy as a mechanism towards making a liquid metal beating heart. *RSC Adv.* **2016**, *6*, 94692−94698.
(44) Tang, S.-Y.; Joshipura, I. D.; Lin, Y.; Kalantar-Zadeh, K.; Mitchell, A.; Khoshmanesh, K.; Dickey, M. D. Liquid-Metal Microdroplets Formed Dynamically with Electrical Control of Size and Rate. *Adv. Mater.* **2016**, *28*, 604−609.
(45) He, J.; Shi, F.; Wu, J.; Ye, J. Shape Transformation Mechanism of Gallium−Indium Alloyed Liquid Metal Nanoparticles. *Adv. Mater. Interfaces* **2021**, *8*, 2001874.
(46) Qian, H.-S.; Gunawan, P.; Zhang, Y.-X.; Lin, G.-F.; Zheng, J.-W.; Xu, R. Template-Free Synthesis of Highly Uniform α-GaOOH Spindles and Conversion to α-Ga2O3 and β-Ga2O3. *Cryst. Growth Des.* **2008**, *8*, 1282−1287.
(47) Huang, C.-C.; Yeh, C.-S.; Ho, C.-J. Laser Ablation Synthesis of Spindle-like Gallium Oxide Hydroxide Nanoparticles with the Presence of Cationic Cetyltrimethylammonium Bromide. *J. Phys. Chem. B* **2004**, *108*, 4940−4945.
(48) Zhao, Y.; Frost, R. L.; Yang, J.; Martens, W. N. Size and Morphology Control of Gallium Oxide Hydroxide GaO(OH), Nano- to Micro-Sized Particles by Soft-Chemistry Route without Surfactant. *J. Phys. Chem. C* **2008**, *112*, 3568−3579.
(49) Klug, A.; Farkas, L. Structural investigations of polycrystalline diaspore samples by X-ray powder diffraction. *Phys. Chem. Miner.* **1981**, *7*, 138−140.
(50) Markov, I. *Crystal Growth for Beginners: Fundamentals of Nucleation, Crystal Growth and Epitaxy*; World Scientific, 1995; p 15.

https://doi.org/10.1021/acsomega.1c06897
ACS Omega 2022, 7, 7912−7919